Acta Crystallographica Section D
Biological Crystallography
ISSN 0907-4449

Structure determination from a single high-pressure-frozen virus crystal

Anja Burkhardt,[a] Armin Wagner,[b] Martin Warmer,[c] Rudolph Reimer,[c] Heinrich Hohenberg,[c] Jingshan Ren,[d] Elizabeth E. Fry,[d] David I. Stuart[b,d] and Alke Meents[a]*

[a]Deutsches Elektronen-Synchrotron (DESY), Notkestrasse 85, 22607 Hamburg, Germany, [b]Diamond Light Source, Chilton, Didcot, Oxfordshire OX11 0DE, England, [c]Heinrich Pette Institute, Leibniz Institute for Experimental Virology, Martinistrasse 52, 20251 Hamburg, Germany, and [d]Division of Structural Biology, University of Oxford, The Henry Wellcome Building for Genomic Medicine, Headington, Oxford OX3 7BN, England

Correspondence e-mail: alke.meents@desy.de

Received 22 August 2012
Accepted 2 November 2012

Successful cryogenic X-ray structure determination from a single high-pressure-frozen bovine enterovirus 2 crystal is reported. The presented high-pressure-freezing procedure is based on a commercially available device and allows the cryocooling of macromolecular crystals directly in their mother liquor without the time- and crystal-consuming search for optimal cryoconditions. The method is generally applicable and will allow cryogenic data collection from all types of macromolecular crystals.

1. Introduction

A major limitation to successful crystal structure determination in macromolecular crystallography (MX), especially for large molecular complexes, is X-ray-induced radiation damage (Blake & Phillips, 1962). Cryocooling to 100 K and below can drastically reduce the detrimental effects of radiation damage (Garman & Owen, 2006; Meents *et al.*, 2010; Rodgers, 1994). Macromolecular crystals typically contain 30–90% solvent (predominantly water) in channels and are surrounded by their mother liquor. Direct cooling of these crystals leads to the formation of hexagonal ice, which disrupts the crystal lattice. Successful cryocooling of macromolecular crystals therefore requires the conversion of the water to amorphous ice, also referred to as vitrification.

In MX, vitrification is normally achieved by exposing the crystals to penetrating cryoprotectants such as glycerol or ethylene glycol prior to flash-cooling (Garman & Schneider, 1997; Hope, 1988). However, finding optimal cryoconditions is often challenging and time-consuming and can require a large number of crystals. Even though successful cryoprotection of systems with weak crystal contacts such as viruses has been reported in several cases (see, for example, Gan *et al.*, 2006; Nam *et al.*, 2007; Xiao *et al.*, 2005), there are many systems for which it has proved impossible to find suitable cryoconditions and many experiments are still performed at room temperature. Inspection of the VIPER database (http://viperdb.scripps.edu) indicates that the large majority of virus structures have been determined at room temperature (Carrillo-Tripp *et al.*, 2009).

The same problem occurs in the cryo-electron microscopy (cryo-EM) of biological samples. Here, cooling to cryogenic temperatures is required to work under vacuum conditions and also to reduce radiation damage as in the case of macromolecular crystals. Similar to those in MX, cryo-EM samples also possess a high water content, but cryoprotectants are preferably avoided as they can alter the structure of the samples. A commonly applied technique in biological cryo-EM is high-pressure-freezing (HPF). HPF does not require any cryoprotectants and allows vitrification of the samples in their native state (Moor, 1971). For HPF, samples are first pressurized to 210 MPa and then immediately cooled to 77 K with liquid nitrogen (Hohenberg *et al.*, 1994; Studer *et al.*, 1995, 2008). Using this technique, cooling rates of up to 7000 K s^{-1} can be achieved (Shimoni & Müller, 1998).

HPF was introduced to MX in 1973 (Thomanek *et al.*, 1973) and was further developed by Kim *et al.* (2005). In contrast to the method routinely applied in cryo-EM, the protocol involves slow pressurization and cooling rates below 2 K s^{-1} (Urayama *et al.*, 2002). Structures of several protein crystals have been determined using this approach (Albright *et al.*, 2006; Barstow *et al.*, 2008; Chen *et al.*, 2009; Collins *et al.*, 2005, 2011; Domsic *et al.*, 2008; Kim *et al.*, 2006).

However, the successful HPF of challenging systems such as viruses has not been reported until now.

Recently, an alternative approach for HPF of macromolecular crystals was developed by our group and subsequently by Kurz and coworkers (Burkhardt *et al.*, 2012; Kurz *et al.*, 2012). Our method involves surface-cooling rates of 3×10^3 to 2×10^4 K s^{-1}, which are typically required for vitrification of biological samples using a commercially available device (Bald, 1986; Riehle, 1968). It was the goal of the present work to determine whether this protocol can be applied to sensitive crystals of a large unit-cell system with weak crystal contacts, for which often no cryoconditions can be established.

2. Experimental

2.1. Crystal growth

Crystals of bovine enterovirus 2 (BEV2; grown and purified in the Department of Microbiology, University of Leeds by Professor D. Rowlands) were grown from virus at a concentration of 7 mg ml^{-1} in 96-well Greiner CrystalQuick SW and CrystalQuick X plates using a Cartesian robot (Walter *et al.*, 2005). The trays were sealed with Greiner VIEWseal tape and stored at 293.5 K. Crystals of bipyramidal morphology grew in many conditions from the SaltRx screen (Hampton Research) which did not contain any cryoprotectant (Axford *et al.*, 2012).

2.2. High-pressure-freezing

Sample preparation, high-pressure-freezing and subsequent sample manipulation were performed as reported previously (Burkhardt *et al.*, 2012). BEV2 crystals with dimensions of less than 50 µm were drawn into thin-walled glass capillaries with an inner diameter of ∼110 µm (see Fig. 1). The capillaries containing the virus crystals were cut into smaller pieces, sandwiched between two aluminium platelets and then subjected to HPF using a Baltec HPM 010 device (for a more detailed description, see Dahl & Staehelin, 1989). After HPF, the sample was immediately transferred into a liquid-nitrogen bath. Further sample manipulation was performed in an AFS2 freeze substitution device (Leica) at cryogenic temperatures below 135 K. Unlike in previous experiments, the capillary segments

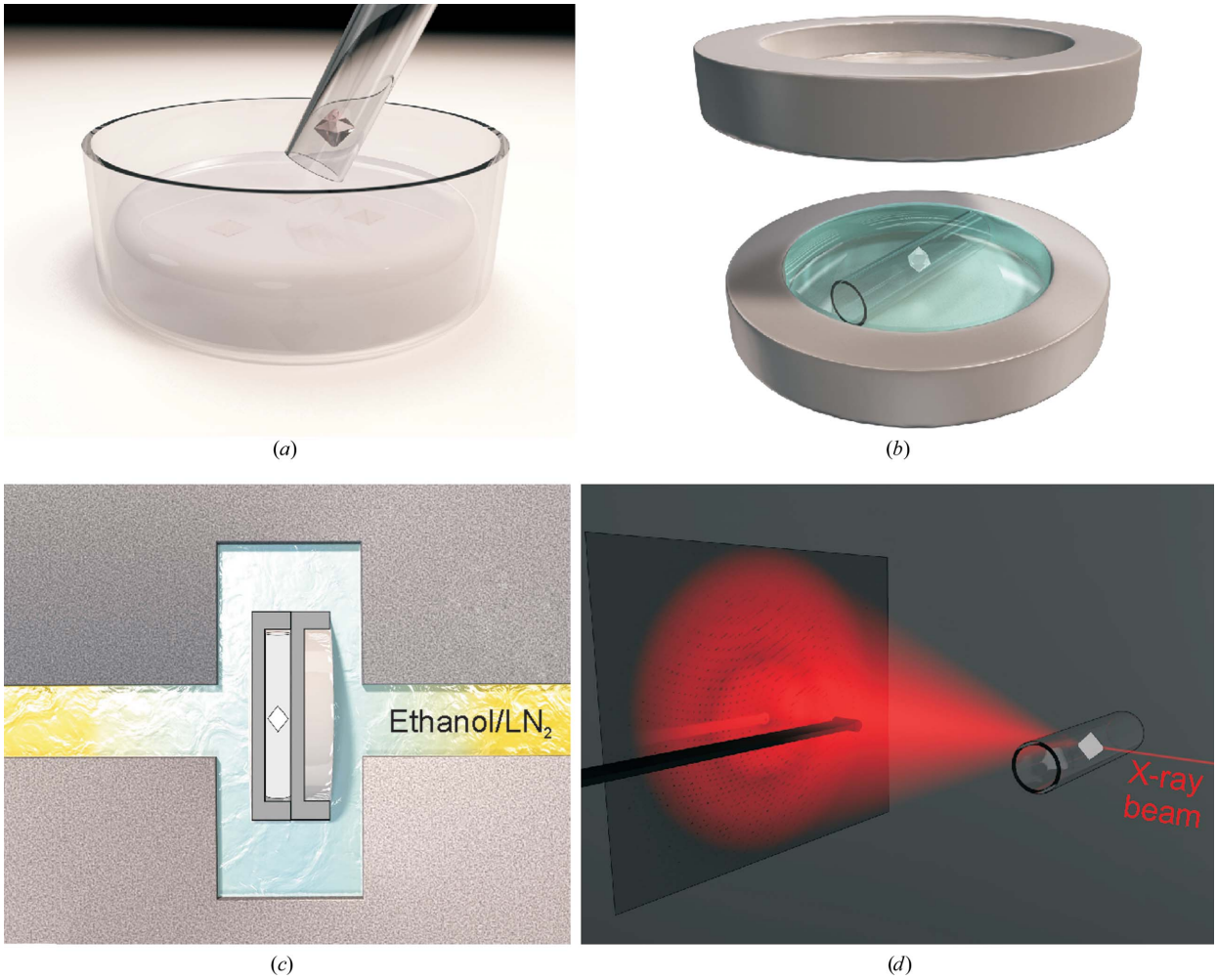

Figure 1
Experimental setup from sample preparation to data collection. (*a*) Crystals grown by sitting-drop vapour diffusion are drawn into thin-walled quartz capillaries. (*b*) The capillary containing the crystal in its mother liquor is cut to ∼2 mm in length and transferred to an aluminium platelet. The cavity of the platelet is completely filled with 1-hexadecene. The platelet is sandwiched with an aluminium lid and this containment is inserted to the pressure chamber of the Baltec HPM 010 device. (*c*) The pressure chamber is automatically filled with ethanol at room temperature. Subsequently, liquid nitrogen (LN_2) pressurized to 210 MPa is 'shot' onto both sides of the sample containment *via* a jet. Using this procedure, the sample is rapidly cooled to liquid-nitrogen temperature immediately after pressurization (for further details, see Dahl & Staehelin, 1989). (*d*) For X-ray data collection the sample is removed from the containment. The capillary containing the frozen crystal is mounted on a steel pin so that it is oriented perpendicular to the incident X-ray beam. All of these sample-handling procedures are performed at cryogenic temperatures.

were inserted at one end into a hollow steel pin with an inner diameter of 210 µm and fixed. The steel pin itself was mounted on a standard magnetic crystal cap (Hampton Research).

2.3. Data collection, data processing and structure refinement

Diffraction data from the HPF BEV2 crystal were collected on the micro-focus beamline I24 at the Diamond Light Source (DLS), Didcot, England using a Pilatus 6M detector (Dectris, Switzerland). A total of 150 images were collected using an X-ray wavelength of 0.9686 Å, a rotation range of 0.2° per image and an exposure time of 0.2 s per frame. The crystal-to-detector distance was 450 mm. The beamsize was adjusted to 10 × 10 µm. Diffraction data were collected at 100 K using an open-flow nitrogen cryostat. Data collection from cryoprotected BEV2 crystals was performed on beamline I03 at DLS (Table 1).

Diffraction data at room temperature (293.5 K) were also collected on beamline I24 using a Pilatus 6M detector. A total of 326 images were collected from 28 crystals at 76 crystal positions using an X-ray wavelength of 0.9778 Å, a rotation range of 0.1° per image and an exposure time of 0.1 s per frame. The crystal-to-detector distance was 482 or 530 mm. The beamsize was adjusted to 20 × 20 µm.

Data frames were indexed and integrated with *HKL*-2000 and scaled with *SCALEPACK* (Otwinowski & Minor, 1997). Structure refinements were performed with *CNS* using strict fivefold NCS constraints (Brünger *et al.*, 1998).

3. Results and discussion

We describe the first successful structure determination from high-pressure-frozen virus crystals. We have developed a protocol which allows high-pressure-freezing at high cooling rates using a commercially available HPF device (Baltec HPM 010). Crystals of bovine enterovirus 2 (BEV2), a virus requiring no disease precautions, were grown by sitting-drop vapour diffusion (Walter *et al.*, 2005). The BEV2 crystals belonged to space group *F*23, with unit-cell parameter

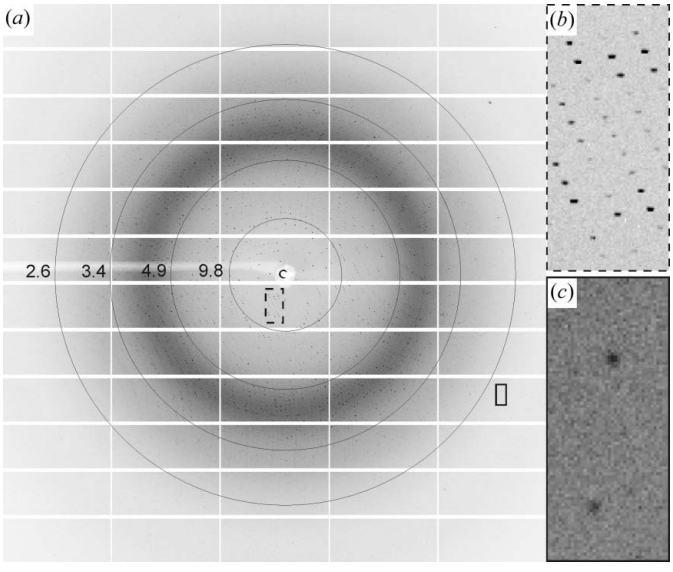

Figure 2
Diffraction data collected from an HPF BEV2 crystal on the micro-focus beamline I24 at the Diamond Light Source (rotation increment 0.2°). (*a*) Overall diffraction image. (*b*) Enlargement showing low-resolution data between 11.4 and 27.1 Å resolution [rectangle with dashed line in (*a*)]. (*c*) Enlargement showing high-resolution data around 2.4 Å resolution [rectangle with solid line in (*a*)].

Table 1
Data-collection and refinement statistics.

Values in parentheses are for the highest resolution shell.

	HPF	RT	CP†
Data collection			
Crystal size (µm)	30 × 30 × 30	50 × 50 × 50 to 100 × 100 × 100	50 × 50 × 50
Temperature (K)	100	293.5	100
Unit-cell parameter (Å)	*a* = 432.5	*a* = 436.6	*a* = 426.5
Space group	*F*23	*F*23	*F*23
Resolution (Å)	50.0–2.50 (2.59–2.50)	50.0–2.10 (2.18–2.10)	50.0–4.00 (4.14–4.00)
No. of observed reflections	281645	592107	163227
No. of unique reflections	163062	260688	47613
R_{merge} (%)	27.5 (—)	19.6 (40.4)	36.7 (—)
Completeness (%)	71.6 (74.4)	65.8 (17.2)	88.6 (91.5)
$\langle I/\sigma(I)\rangle$	2.2 (0.5)	4.3 (1.2)	2.6 (0.7)
Multiplicity	1.7 (1.6)	2.3 (1.2)	3.4 (3.3)
Mosaic spread (°)	0.26	∼0.04	∼0.70
Refinement			
Resolution range (Å)	50–2.50	50–2.10	
No. of reflections	157703	247641	
No. of protein residues	6224	6224	
No. of ligand molecules	42	42	
No. of water molecules	267	289	
R.m.s.d. bond lengths (Å)	0.010	0.012	
R.m.s.d. bond angles (°)	1.6	1.7	
R_{work} (%)	22.7	19.6	
R_{free}‡ (%)	23.5	20.7	
Average *B* factors (Å^2)			
Protein atoms	26	17	
Ligand atoms	47	35	
Water molecules	35	26	
Average particle radius (Å)	127.7	128.9	

† Cryoprotected. ‡ R_{free} was calculated from 1% of the data that were randomly chosen and omitted from refinement; however, it is of limited significance owing to the considerable noncrystallographic symmetry.

a = 436.6 Å at room temperature. Initial attempts to cryoprotect these BEV2 crystals using several standard procedures with glycerol, ethylene glycol and paraffin oil failed to yield useful diffraction data owing to an increase in the mosaic spread and a dramatic decrease in the resolution of diffraction (from 2.1 Å at room temperature to no better than 4.0 Å at cryogenic temperatures; Table 1).

Fig. 1 shows our experimental setup for data collection from frozen crystals, including sample preparation, HPF and X-ray diffraction measurements.

HPF BEV2 crystals diffracted to reasonable resolution with clearly separated diffraction spots (Fig. 2) and possessed mosaic spreads of about 0.26°. This is much smaller than that observed for conventionally cryoprotected crystals and sufficiently small as to not impede data collection from crystals with large unit cells as in our case. Using a focused beamsize of 10 × 10 µm, the crystals could withstand the unattenuated X-ray beam for about 12 s before showing severe signs of radiation damage. A data set obtained from one single crystal of 30 µm in all dimensions was used for subsequent crystal structure refinement.

For direct comparison, room-temperature (RT) diffraction data were collected from BEV2 crystals on the same beamline. At room temperature the crystal lifetime with a less focused beam of 20 × 20 µm varied between 0.4 and 0.6 s. A total of 326 diffraction images were collected at 76 different crystal positions from 28 individual crystals with sizes between 50 and 100 µm by *in situ* diffraction from a single crystallization plate (Axford *et al.*, 2012). Note that these crystals were significantly larger (on average about twice as large in each direction) than that subjected to HPF. All room-temperature diffraction images were merged into one data set for structure refinement. Data-collection parameters and refinement statistics of both the HPF crystal data set and the merged RT data set are

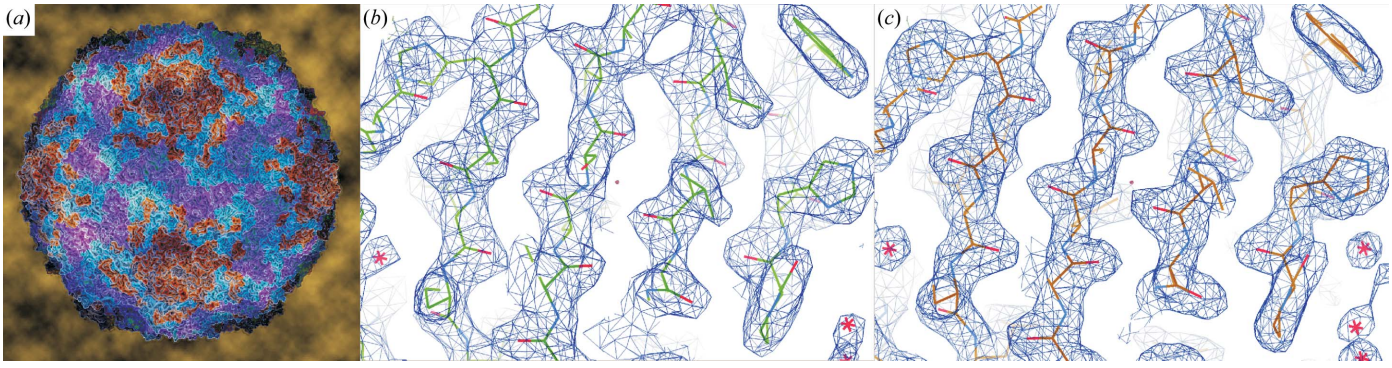

Figure 3
Overall structure and electron-density maps of BEV2. (*a*) Surface representation of HPF BEV2 as viewed down the icosahedral twofold axis. (*b*, *c*) Single-cycle averaged electron-density maps contoured at 2σ showing the same region of the virus from the high-pressure-frozen crystal measured at 100 K (*b*) and from data collected at 293.5 K (*c*).

summarized in Table 1. For direct comparison of HPF with conventional cryoprotection (CP), Table 1 also shows low-temperature data from a crystal cryoprotected with 25% glycerol. Owing to the poor diffraction properties of the crystal, structure refinement was not possible.

Fig. 3(*a*) shows the electron density obtained from a single high-pressure-frozen BEV2 crystal. The HPF and RT structures are very similar at the detailed level (r.m.s. deviation of 0.29 Å in C^{α} atoms when the complete icosahedral asymmetric units are superposed as a single rigid body), although there is an ∼1% shrinkage in the unit cell and in the overall size of the virus particle on cooling (Table 1). The electron-density maps possess similar features and are of comparable quality (Figs. 3*b* and 3*c*).

Overall, the quality of the data is similar despite the HPF data being recorded at a single position from one crystal rather than at 76 positions from 28 larger crystals as in the case of the room-temperature measurements. Taking the fourfold higher flux density and the smaller dimensions of the HPF crystal into account, the 'gain factor' in radiation tolerance for data collection at 100 K compared with room-temperature measurements is more than 100 in our case.

In this work, we demonstrate successful HPF of virus crystals for the first time. HPF is very well suited to the successful cryocooling of large unit-cell systems such as BEV2. All of the equipment used in this study is commercially available and there is still great scope for optimizing the logistics of sample handling and data collection to improve the quality of the HPF data and the success rate of the method. Not only is data collection feasible from far fewer crystals, but for large viruses, for which only a single image can be recorded per crystal at room temperature, this approach will increase the effective resolution obtainable and is likely to render some otherwise almost impossible projects tractable (Abrescia *et al.*, 2004, 2008).

Our virus crystals were directly frozen from their mother liquor without the need for any penetrative cryoprotectants. This makes HPF a method that is useful not only for the special case of virus crystallography but also for challenging problems in macromolecular crystallography in general. HPF will allow cryogenic data collection from all macromolecular crystals independent of their growth conditions. This method should have a large impact as it allows data collection from frozen crystals without the time-consuming and also crystal-consuming search for optimal cryoconditions.

We would like to thank Professor D. Rowlands (University of Leeds) for providing samples of BEV2. DIS and EEF are supported by the MRC and JR by the Wellcome Trust. M. Holthaus is acknowledged for providing illustrations of the HPF setup.

References

Abrescia, N. G., Cockburn, J. J., Grimes, J. M., Sutton, G. C., Diprose, J. M., Butcher, S. J., Fuller, S. D., San Martín, C., Burnett, R. M., Stuart, D. I., Bamford, D. H. & Bamford, J. K. (2004). *Nature (London)*, **432**, 68–74.
Abrescia, N. G., Grimes, J. M., Kivelä, H. M., Assenberg, R., Sutton, G. C., Butcher, S. J., Bamford, J. K., Bamford, D. H. & Stuart, D. I. (2008). *Mol. Cell*, **31**, 749–761.
Albright, R. A., Ibar, J. L., Kim, C. U., Gruner, S. M. & Morais-Cabral, J. H. (2006). *Cell*, **126**, 1147–1159.
Axford, D. *et al.* (2012). *Acta Cryst.* D**68**, 592–600.
Bald, W. B. (1986). *J. Microsc.* **143**, 89–102.
Barstow, B., Ando, N., Kim, C. U. & Gruner, S. M. (2008). *Proc. Natl Acad. Sci. USA*, **105**, 13362–13366.
Blake, C. F. F. & Phillips, D. C. (1962). *Biological Effects of Ionizing Radiation at the Molecular Level*, pp. 183–191. Vienna: IAEA.
Brünger, A. T., Adams, P. D., Clore, G. M., DeLano, W. L., Gros, P., Grosse-Kunstleve, R. W., Jiang, J.-S., Kuszewski, J., Nilges, M., Pannu, N. S., Read, R. J., Rice, L. M., Simonson, T. & Warren, G. L. (1998). *Acta Cryst.* D**54**, 905–921.
Burkhardt, A., Warmer, M., Panneerselvam, S., Wagner, A., Zouni, A., Glöckner, C., Reimer, R., Hohenberg, H. & Meents, A. (2012). *Acta Cryst.* F**68**, 495–500.
Carrillo-Tripp, M., Shepherd, C. M., Borelli, I. A., Venkataraman, S., Lander, G., Natarajan, P., Johnson, J. E., Brooks, C. L. & Reddy, V. S. (2009). *Nucleic Acids Res.* **37**, D436–D442.
Chen, Y.-F., Tate, M. W. & Gruner, S. M. (2009). *J. Appl. Cryst.* **42**, 525–530.
Collins, M. D., Hummer, G., Quillin, M. L., Matthews, B. W. & Gruner, S. M. (2005). *Proc. Natl Acad. Sci. USA*, **102**, 16668–16671.
Collins, M. D., Kim, C. U. & Gruner, S. M. (2011). *Annu. Rev. Biophys.* **40**, 81–98.
Dahl, R. & Staehelin, L. A. (1989). *J. Electron Microsc. Tech.* **13**, 165–174.
Domsic, J. F., Avvaru, B. S., Kim, C. U., Gruner, S. M., Agbandje-McKenna, M., Silverman, D. N. & McKenna, R. (2008). *J. Biol. Chem.* **283**, 30766–30771.
Gan, L., Speir, J. A., Conway, J. F., Lander, G., Cheng, N., Firek, B. A., Hendrix, R. W., Duda, R. L., Liljas, L. & Johnson, J. E. (2006). *Structure*, **14**, 1655–1665.
Garman, E. F. & Owen, R. L. (2006). *Acta Cryst.* D**62**, 32–47.
Garman, E. F. & Schneider, T. R. (1997). *J. Appl. Cryst.* **30**, 211–237.
Hohenberg, H., Mannweiler, K. & Müller, M. (1994). *J. Microsc.* **175**, 34–43.
Hope, H. (1988). *Acta Cryst.* B**44**, 22–26.
Kim, C. U., Hao, Q. & Gruner, S. M. (2006). *Acta Cryst.* D**62**, 687–694.
Kim, C. U., Kapfer, R. & Gruner, S. M. (2005). *Acta Cryst.* D**61**, 881–890.
Kurz, M., Blattmann, B., Kaech, A., Briand, C., Reardon, P., Ziegler, U. & Gruetter, M. G. (2012). *J. Appl. Cryst.* **45**, 999–1008.
Meents, A., Gutmann, S., Wagner, A. & Schulze-Briese, C. (2010). *Proc. Natl Acad. Sci. USA*, **107**, 1094–1099.
Moor, H. (1971). *Philos. Trans. R. Soc. Lond. B*, **261**, 121–131.

Nam, H.-J., Lane, M. D., Padron, E., Gurda, B., McKenna, R., Kohlbrenner, E., Aslanidi, G., Byrne, B., Muzyczka, N., Zolotukhin, S. & Agbandje-McKenna, M. (2007). *J. Virol.* **81**, 12260–12271.
Otwinowski, Z. & Minor, W. (1997). *Methods Enzymol.* **276**, 307–326.
Riehle, U. (1968). *Chem. Ing. Tech.* **40**, 213–218.
Rodgers, D. W. (1994). *Structure*, **2**, 1135–1140.
Shimoni, E. & Müller, M. (1998). *J. Microsc.* **192**, 236–247.
Studer, D., Humbel, B. M. & Chiquet, M. (2008). *Histochem. Cell Biol.* **130**, 877–889.
Studer, D., Michel, M., Wohlwend, M., Hunziker, E. B. & Buschmann, M. D. (1995). *J. Microsc.* **179**, 321–332.
Thomanek, U. F., Parak, F., Mössbauer, R. L., Formanek, H., Schwager, P. & Hoppe, W. (1973). *Acta Cryst.* A**29**, 263–265.
Urayama, P., Phillips, G. N. & Gruner, S. M. (2002). *Structure*, **10**, 51–60.
Walter, T. S. *et al.* (2005). *Acta Cryst.* D**61**, 651–657.
Xiao, C., Bator-Kelly, C. M., Rieder, E., Chipman, P. R., Craig, A., Kuhn, R. J., Wimmer, E. & Rossmann, M. G. (2005). *Structure*, **13**, 1019–1033.